PHYSICAL REVIEW B **87**, 241101(R) (2013)

Formation of orbital-selective electron states in $LaTiO_3/SrTiO_3$ superlattices

Frank Lechermann,[1] Lewin Boehnke,[1] and Daniel Grieger[2]
[1]*I. Institut für Theoretische Physik, Universität Hamburg, D-20355 Hamburg, Germany*
[2]*International School for Advanced Studies (SISSA), and CNR-IOM Democritos, Via Bonomea 265, I-34136 Trieste, Italy*
(Received 7 April 2013; published 5 June 2013)

The interface electronic structure of correlated $LaTiO_3/SrTiO_3$ superlattices is investigated by means of the charge self-consistent combination of the local density approximation (LDA) to density functional theory with dynamical mean-field theory. Utilizing a pseudopotential technique together with a continuous-time quantum Monte Carlo approach, the resulting complex multiorbital electronic states are addressed in a coherent fashion beyond static mean field. General structural relaxations are taken into account on the LDA level and cooperate with the driving forces from strong electronic correlations. This alliance leads to a Ti($3d_{xy}$) dominated low-energy quasiparticle peak and a lower Hubbard band in line with photoemission studies. Furthermore correlation effects close to the band-insulating bulk $SrTiO_3$ limit as well as the Mott-insulating bulk $LaTiO_3$ limit are studied via realistic single-layer embeddings.

DOI: 10.1103/PhysRevB.87.241101 PACS number(s): 73.20.−r, 71.27.+a, 71.15.−m

The research on layered heterostructures composed of different metal oxide (MO) compounds has emerged as a major new field in condensed matter physics.[1] Especially the intriguing appearance of a two-dimensional (2D) electron gas from interfacing bulk-insulating MOs may open the door for new tailored hybrid materials with specific transport, magnetic, and/or superconducting properties. Albeit various such layered MO combinations are realized, heterostructures built up by interlacing band-insulating with Mott-insulating compounds are particularly appealing. As they raise questions about the electronic states resulting from conceptually quite different limits, this structural setup challenges the existing modern first-principles approaches to electronic structure.

Coherent superlattices (SLs) of the strongly correlated $LaTiO_3$ (LTO) Mott insulator with the $SrTiO_3$ (STO) band insulator belong to the most prominent examples of these structured materials.[2] Not only is the LTO/STO interface metallicity displayed; also magnetic correlations are vital due to the antiferromagnetic ordering of LTO[3] below $T_N = 146$ K. Moreover 2D superconductivity has been revealed.[4] Aside from possible polarization mechanisms[5] and suppressing Mott correlations, the nominal Ti^{3+} valence in LTO allows for doping the band-insulating STO side, giving rise to metallic transport. Yet in reality strong Coulomb interactions among the electrons complicate this simplistic picture. Photoemission experiments[6] indeed reveal strong correlation signatures, i.e., lower Hubbard band and quasiparticle (QP) peak, in the valence spectrum. The interface conductivity[7] as well as the optical response[8] is identified as dependent on electronic correlations. Numerous theoretical studies on the interface electronic structure exist. There are initial tailored Hubbard-model considerations from unrestricted Hartree-Fock,[9] several first-principles investigations based on Kohn-Sham density functional theory (DFT),[10–12] and DFT + U studies,[13,14] as well as many-body approaches based on the Lanczos-method,[15] slave bosons,[16] and dynamical mean-field theory (DMFT).[17,18]

Contrary to former studies, this work treats the effective single-particle character of the materials' chemistry on an equal footing with many-body effects from a local perspective. We performed charge self-consistent DFT + DMFT[19,20] computations for selected LTO/STO SLs that allow for detailed examinations of the subtle interplay between realistic interface effects and multiorbital electronic correlations at room temperature. It is revealed that structural relaxations and electronic correlations ally in driving an enlarged Ti($3d_{xy}$) orbital polarization in real space *and* in the low-energy spectrum. Fostered by enlarged lateral coherency effects, a prominent renormalized d_{xy} QP peak resides close to the Fermi level. Moreover investigated single-layer LTO/STO architectures remain metallic throughout the SLs.

The theoretical approach (see Refs. 21 and 22 for details) builds up on the combination of a mixed-basis pseudopotential framework[23] with a hybridization-expansion continuous-time quantum Monte Carlo solver[24–26] for the DMFT impurity problem. To include important structural relaxations[11–13] in a general scope, allowing for layer-distance variation *and* tilting of the TiO_6 octahedra, we constructed SLs in an $(n,m) \times 2$ setup, where n,m denote the numbers of LaO, SrO layers in the unit cell with two in-plane Ti ions, respectively (see Fig. 1). The two Ti ions are assumed equivalent by symmetry in each layer, so possible lateral orderings[14] are suppressed. For all discussed SLs the lateral lattice constant was set to the STO value $a = 3.905$ Å and a ratio $c/a = 0.99$ was identified reasonable.

Figure 1 shows the LDA band structure for a $(4,4) \times 2$ superlattice (80-atom unit cell) along with the density of states (DOS). The occupied bands just below the Fermi level ε_F with dominant Ti(t_{2g}) character accommodate the eight additional electrons from the La^{3+} ions in the unit cell. Structural relaxations, relevant also in the STO part, enlarge the gap between the O($2p$)-derived bands deep in energy and the latter t_{2g} bands as well as increase the pseudogap between t_{2g}- and e_g-like states high in energy. A DOS maximum right at ε_F exists for both structural cases, but there is a gain of 36 meV/atom in the LDA total energy upon relaxation. The real-space distribution of the occupied t_{2g} valence charge density in Fig. 1 elucidates the t_{2g} doping in the STO part. This charge transfer is even strengthened in the relaxed orthorhombic structure.

The $(4,4) \times 2$ unit cell contains five symmetry inequivalent Ti ions, denoted here Ti1–5, of which the local t_{2g} DOS from projected local orbitals[21] is displayed in Fig. 2(b). From the

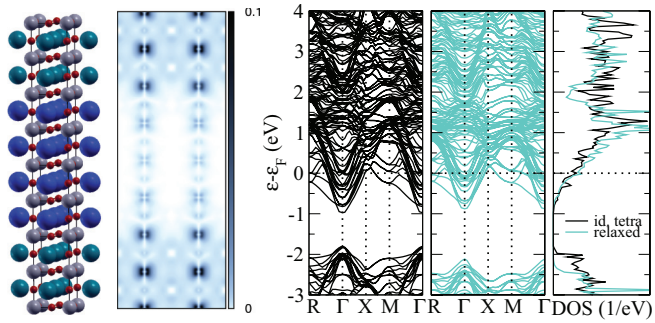

FIG. 1. (Color online) Left: $(4,4) \times 2$ $LaTiO_3/SrTiO_3$ ideal tetragonal unit cell with La (big green/gray), Sr (big blue/dark), Ti (gray/light gray), and O (small red/dark) ions as well as the charge density from t_{2g}-like LDA bands below ε_F, holding $8\,e^-$. Right: Corresponding LDA band structure and DOS for ideal-tetragonal and orthorhombic-relaxed case.

mid-LTO part (Ti1) to the mid-STO part (Ti5) the t_{2g} filling is decreasing. The effective bandwidth shrinks from ∼4 eV down to ∼2.5 eV, with minor smaller size in the relaxed structure. Though overall rather balanced, the d_{xy} occupation is somewhat increased by structural relaxation. In the latter case, the total number of t_{2g} electrons is higher, i.e., the doping of these states is more efficient.

To capture the effect of many-body correlations an effective three-orbital Hubbard Hamiltonian $\mathcal{H}$ with fully rotational invariant interaction terms, i.e.,

$$\mathcal{H} = U \sum_m n_{m\uparrow} n_{m\downarrow} + \frac{1}{2} \sum_{m \neq m',\sigma} \{U' n_{m\sigma} n_{m'\bar{\sigma}} + U'' n_{m\sigma} n_{m'\sigma} + J(c^\dagger_{m\sigma} c^\dagger_{m'\bar{\sigma}} c_{m\bar{\sigma}} c_{m'\sigma} + c^\dagger_{m\sigma} c^\dagger_{m\bar{\sigma}} c_{m'\bar{\sigma}} c_{m'\sigma})\}, \quad (1)$$

is applied at each individual Ti site i. It is parametrized by the adequate[27,28] Coulomb integral $U = 5$ eV and the Hund's exchange $J = 0.7$ eV with $U' = U - 2J$ and $U'' = U - 3J$. Including symmetry, this leads to five inequivalent single-site impurity problems embedded in the full charge self-consistent DFT + DMFT calculations for the $(4,4) \times 2$ unit cell. Charge self-consistency is a vital methodological ingredient because of the subtle electron transfers (cf. Fig. 1). For the projected-local-orbital construction of the correlated subspace a number of 80 Kohn-Sham bands starting from the bottom of the t_{2g}-like manifold was used. The double-counting correction applied to each Ti impurity self-energy Σ_i amounts to a site-averaged fully localized[29] term. All DFT + DMFT computations were performed at $T = 290$ K.[30]

In Fig. 2(c) the resulting local t_{2g} spectral functions are plotted. Compared to LDA the total filling increases once more with correlations. Close to the interface especially the d_{xy} orbital character gains further occupation with correlations. Moreover the d_{xy} weight near ε_F is now pronounced compared to $d_{xz,yz}$, resulting in a dominant d_{xy} QP peak below the Fermi level. Coherent transport is thus d_{xy} dominated. From the incoherent high-energy part, the correlation strength is larger in the structurally relaxed orthorhombic SLs. Right at the interface (Ti3 ion) the d_{xy} local spectral part is susceptible to (pseudo)gapping. The site- and orbital-resolved QP weight $Z_{im} = (1 - \partial \Sigma_{im}/\partial \omega)^{-1}$ varies significantly across the interface, revealing somewhat stronger mass renormalization for d_{xy}. The complete DFT + DMFT t_{2g}-like spectral function in Bloch space carries the dominance of the d_{xy} close to the Fermi level (see Fig. 3). While in the unrelaxed tetragonal case a maximum at ε_F remains as in LDA, a minimum occurs when including structural relaxations. Increased spectral-weight transfer towards the lower Hubbard band takes place in the latter. This Hubbard peak shifts closer to −1 eV with relaxations, in good agreement with photoemission.[6]

In order to obtain deeper insight in the relevance of correlation effects, let us turn now to the limiting case of a single LaO (SrO) layer within an STO (LTO) host. Within our superlattice approach two different unit cells were chosen, respectively incorporating 4 and 9 host layers. The larger structure amounts to a 100-atom unit cell. While the 4-layer-host case has 5 Ti layers in between the single layers and 3 inequivalent Ti ions, the 9-layer-host structure has 10 Ti layers and 5 inequivalent ones, denoted Ti1–5 with increasing

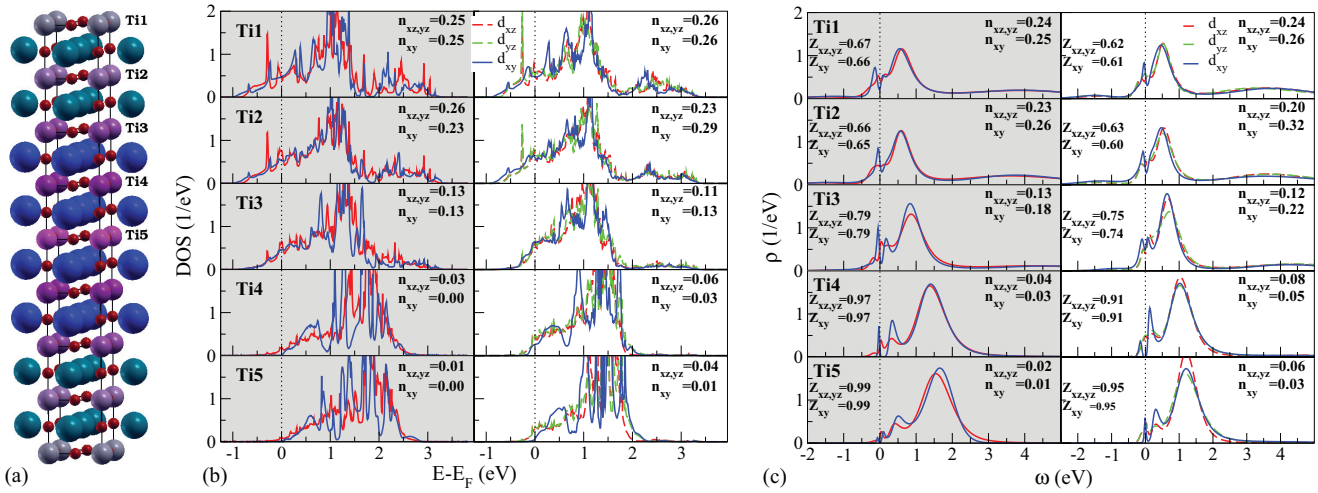

FIG. 2. (Color online) (a) Inequivalent Ti ions for $(4,4) \times 2$. (b) Local Ti1-5 LDA DOS for unrelaxed [gray background (bg)] and structurally relaxed (white bg) cases. (c) Local DFT + DMFT spectral function for Ti1-5 with same color coding. Though $d_{xz,yz}$ are different by symmetry with relaxations, Z and n differ only marginally; hence averaged values are shown.

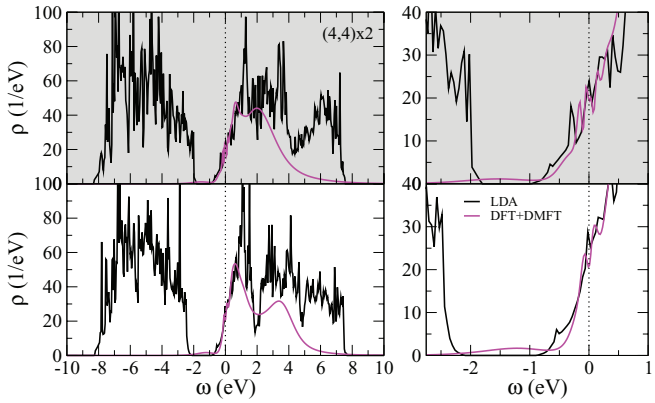

FIG. 3. (Color online) Total t_{2g}-like DFT + DMFT spectral function compared to the LDA DOS for (4,4) × 2. Top: Tetragonal unrelaxed (gray bg), bottom: relaxed orthorhombic (white bg). Right part shows a blow-up close to ε_F.

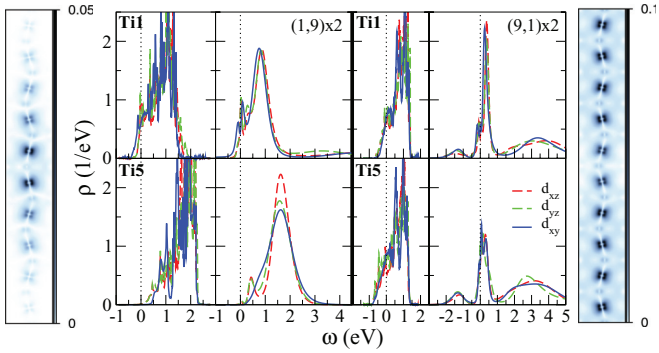

FIG. 5. (Color online) Left: LDA charge density from occupied t_{2g}-like bands for a Ti column along the c axis of (1,9) × 2. Right: Same for (9,1) × 2. Middle: LDA t_{2g}-like DOS (left) and DFT + DMFT spectrum (right) for Ti1, Ti5 (see text).

distance from the threaded single layer. Hence the smaller (larger) structure has an odd (even) number of Ti layers. In the following only the structurally relaxed orthorhombic cases are discussed.

Figure 4 displays the spectral comparison between LDA and charge self-consistent DFT + DMFT applied to the (1,9) × 2 as well as the (9,1) × 2 structure. The correlated spectral function of (1,9) × 2 with one LaO layer in STO is metallic in agreement with optics,[8] showing a smaller QP peak below ε_F and a more prominent one just above. While at low energy the LDA difference between both structural types amounts mainly to a Fermi-level shift (1 vs 9 e^- below ε_F), DFT + DMFT signals the increased correlations for (9,1) × 2 via substantial spectral-weight transfer to Hubbard bands. No insulating state, also not site-selective (see below), is obtained for (9,1) × 2, which thus could be viewed as a doped Mott insulator. Note that also bulk $Sr_{1-x}La_xTiO_3$ is insulating only above $x_c \sim 0.95$.[31] Experiments on confined STO in a larger $GdTiO_3$ host yet show the principle chance for reaching an insulating interface[32] and the finding stimulated modeling ideas based on Hubbard-ladder physics.[33]

Instructive are the local t_{2g}-like occupations for Ti1–5. For the single LaO layer the Ti doping in STO is still not accomplished in (1,4) × 2 far from the interface. But for (1,9) × 2 the Ti5 ion indeed shows zero t_{2g} filling (see also Fig. 5). DFT + DMFT leads here to somewhat farther charge flow into STO and a stronger orbital-filling alignment within the t_{2g} manifold away from the interface. However again the d_{xy} polarization close to it is strengthened with correlations. The evaluated sheet carrier densities (in units of cm^{-2}) $n_{sheet}^{LDA} = 1.8 \times 10^{14}$ and $n_{sheet}^{DFT+DMFT} = 2.3 \times 10^{14}$ agree well with the experimental value $n_{sheet}^{exp} \approx 3 \times 10^{14}$ from optics.[8] The increased charging of the Ti1 ion in DFT + DMFT for the single SrO layer architecture (again favoring d_{xy}) is evident. In general, whereas LDA quickly saturates here to the nominal $n = 1$ t_{2g} occupation, many-body effects result in a balancing of the strong LDA occupation differences with distance from the interface. Even for Ti4, Ti5 the hole doping is vital. A subtle d_{xy}/d_{yz} filling crossover occurs near Ti2, which marks the competition between bulk-LTO Mott-insulating behavior and LTO/STO interface physics. While in the former case indeed the d_{yz} orbital has dominant contribution to the correlated crystal-field ground state,[34] the driving force for d_{xy} polarization is stronger at the interface.

Besides illustrating the real-space variation of the low-energy LDA valence charge density for (9,1) × 2 and (1,9) × 2, in Fig. 5 the local t_{2g}-like spectral properties are visualized for the Ti ions closest (Ti1) and farthest from the single LaO (SrO) layer. The QP structure for Ti1 in (1,9) × 2 is more subtle than for the interface ions in (4,4) × 2, since a strong orbital-selectivity towards d_{xy} has not yet manifested in the single-layer set up. Still a shifting of the large $d_{xz,yz}$ DOS below ε_F towards the unoccupied part is visible. The t_{2g}-like orbitals behave more balanced in (1,9) × 2 with significant Hubbard-band weight for Ti5. However a standard doped-Mott-insulating picturing of the Ti5 multiorbital spectral function seems not applicable; i.e., the QP weight remains sizable.

Finally we want to comment on the energetics of the relaxed embedded single-layer SLs within LDA and DFT + DMFT.[22]

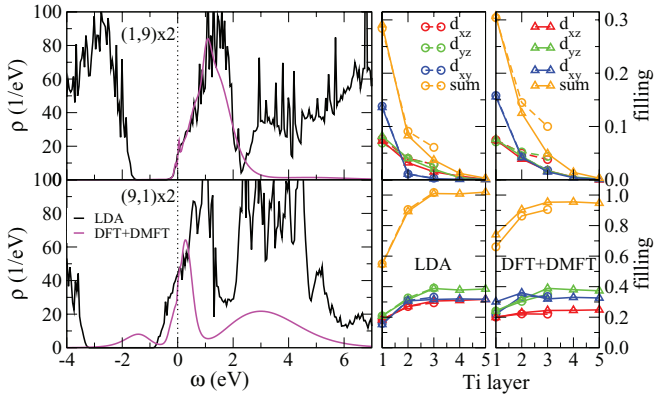

FIG. 4. (Color online) Left: Total t_{2g}-like DFT + DMFT spectral function compared to the LDA DOS for (1,9) × 2 (top) and (9,1) × 2. Right: Ti(t_{2g}) occupations with distance from the LTO/STO layer within LDA (left part) and DFT + DMFT (right part). Circles mark results for the 4-layer host, triangles for the 9-layer host.

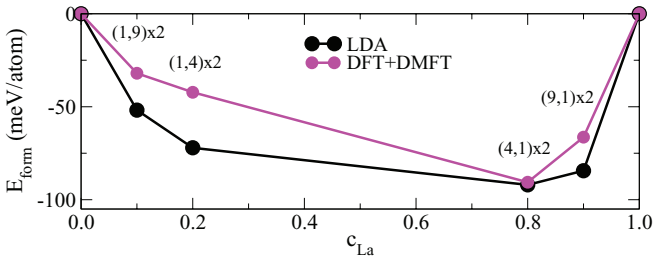

FIG. 6. (Color online) Formation energy and convex hull for the embedded single-layer SLs.

To this we compute the formation energy, defined here as

$$E^{\text{form}}_{n,m} = E^{\text{tot}}_{n,m} - c_{\text{La}} E^{\text{tot}}_{\text{bulk-LTO}} - (1 - c_{\text{La}}) E^{\text{tot}}_{\text{bulk-STO}}, \quad (2)$$

where E^{tot} denotes the total energy per atom and $c_{\text{La}} = n/(n + m)$. Be aware of the nontrivial character, since in the correlated case not only $E^{\text{form}}_{n,m}$ includes many-body corrections but also $E^{\text{tot}}_{\text{LTO,STO}}$. As the projected local orbitals are here derived from t_{2g}-like bands, however, that correction vanishes for bulk STO having those unoccupied. Yet bulk LTO is a Mott insulator in DFT + DMFT,[28] which is verified within the charge self-consistent scheme for the here given many-body Hamiltonian (1), chosen Coulomb parameters, and double counting. Within our double-counting scheme the bulk-LTO correlated Mott state enters Eq. (2) with a much lower total energy. Figure 6 shows the variation of the formation energy based on the four single-layer $(n,m) \times 2$ structures. Already in LDA an asymmetry of the basic convex hull towards the LTO side exists, which is enforced with correlations. Given the delicacy of E^{form}, the values within both theoretical schemes are rather similar, which especially speaks for the novel DFT + DMFT approach to such subtle energetic quantities. The observed trend of generally reduced $E^{\text{form}}_{n,m}$ (though evaluated at finite T) may correct frequent LDA overestimations.

In summary, the correlated electronic structure of realistic LTO/STO SLs has been studied within charge self-consistent DFT + DMFT beyond static mean field. Many-body effects and structural relaxations are revealed to ally in driving orbital-selective behavior towards dominant Ti($3d_{xy}$) filling *and* QP behavior. In addition, significant spectral-weight intensity just above the Fermi level renders intricate susceptibility to applied field possible. Single-layer architectures of these systems result in global, but still intriguing, metallic behavior for the studied embeddings. In general, the recent advances put the DFT + DMFT formalism in position for challenging materials investigations, including engineered systems. A further methodological step will be the sound computation of correlation-influenced structural relaxations. Future DFT + DMFT work on MO heterostructures such as the study of possible ordering instabilities, of different interface geometries, and of spin-orbit effects is envisaged.

Calculations were performed on the JUROPA cluster of the Jülich Supercomputing Centre (JSC). This research was supported by the DFG-FOR1346 project.

[1] H. Y. Hwang, Y. Iwasa, M. Kawasaki, B. Keimer, N. Nagaosa, and Y. Tokura, Nat. Mater. **11**, 103 (2012).
[2] A. Ohtomo, D. A. Muller, J. L. Grazul, and H. Y. Hwang, Nature (London) **419**, 378 (2002).
[3] G. I. Meijer, W. Henggeler, J. Brown, O.-S. Becker, J. G. Bednorz, C. Rossel, and P. Wachter, Phys. Rev. B **59**, 11832 (1999).
[4] J. Biscaras, N. Bergeal, A. Kushwaha, T. Wolf, A. Rastogi, R. C. Budhani, and J. Lesueur, Nat. Commun. **1**, 89 (2010).
[5] N. Nakagawa, H. Y. Hwang, and D. A. Muller, Nat. Mater. **5**, 204 (2006).
[6] M. Takizawa, H. Wadati, K. Tanaka, M. Hashimoto, T. Yoshida, A. Fujimori, A. Chikamatsu, H. Kumigashira, M. Oshima, K. Shibuya, T. Mihara, T. Ohnishi, M. Lippmaa, M. Kawasaki, H. Koinuma, S. Okamoto, and A. J. Millis, Phys. Rev. Lett. **97**, 057601 (2006).
[7] H. W. Jang, D. A. Felker, C. W. Bark, Y. Wang, M. K. Niranjan, C. T. Nelson, Y. Zhang, D. Su, C. M. Folkman, S. H. Baek, S. Lee, K. Janicka, Y. Zhu, X. Q. Pan, D. D. Fong, E. Y. Tsymbal, M. S. Rzchowski, and C. B. Eom, Science **331**, 886 (2011).
[8] S. S. A. Seo, W. S. Choi, H. N. Lee, L. Yu, K. W. Kim, C. Bernhard, and T. W. Noh, Phys. Rev. Lett. **99**, 266801 (2007).
[9] S. Okamoto and A. J. Millis, Nature (London) **428**, 630 (2004).
[10] Z. S. Popovic and S. Satpathy, Phys. Rev. Lett. **94**, 176805 (2005).
[11] D. R. Hamann, D. A. Muller, and H. Y. Hwang, Phys. Rev. B **73**, 195403 (2006).
[12] P. Larson, Z. S. Popović, and S. Satpathy, Phys. Rev. B **77**, 245122 (2008).
[13] S. Okamoto, A. J. Millis, and N. A. Spaldin, Phys. Rev. Lett. **97**, 056802 (2006).
[14] R. Pentcheva and W. E. Pickett, Phys. Rev. Lett. **99**, 016802 (2007).
[15] S. S. Kancharla and E. Dagotto, Phys. Rev. B **74**, 195427 (2006).
[16] A. Rüegg, S. Pilgram, and M. Sigrist, Phys. Rev. B **75**, 195117 (2007).
[17] S. Okamoto and A. J. Millis, Phys. Rev. B **70**, 241104(R) (2004).
[18] H. Ishida and A. Liebsch, Phys. Rev. B **77**, 115350 (2008).
[19] S. Y. Savrasov, G. Kotliar, and E. Abrahams, Nature (London) **410**, 793 (2001).
[20] L. V. Pourovskii, B. Amadon, S. Biermann, and A. Georges, Phys. Rev. B **76**, 235101 (2007).
[21] B. Amadon, F. Lechermann, A. Georges, F. Jollet, T. O. Wehling, and A. I. Lichtenstein, Phys. Rev. B **77**, 205112 (2008).
[22] D. Grieger, C. Piefke, O. E. Peil, and F. Lechermann, Phys. Rev. B **86**, 155121 (2012).
[23] B. Meyer, C. Elsässer, F. Lechermann, and M. Fähnle, FORTRAN 90 Program for Mixed-Basis-Pseudopotential Calculations for Crystals, Max-Planck-Institut für Metallforschung, Stuttgart (unpublished).
[24] A. N. Rubtsov, V. V. Savkin, and A. I. Lichtenstein, Phys. Rev. B **72**, 035122 (2005).
[25] P. Werner, A. Comanac, L. de' Medici, M. Troyer, and A. J. Millis, Phys. Rev. Lett. **97**, 076405 (2006).
[26] M. Ferrero and O. Parcollet, TRIQS: A Toolbox for Research in Interacting Quantum Systems, http://ipht.cea.fr/triqs.
[27] T. Mizokawa and A. Fujimori, Phys. Rev. B **51**, 12880 (1995).

[28]E. Pavarini, S. Biermann, A. Poteryaev, A. I. Lichtenstein, A. Georges, and O. K. Andersen, Phys. Rev. Lett. **92**, 176403 (2004).

[29]I. V. Solovyev, P. H. Dederichs, and V. I. Anisimov, Phys. Rev. B **50**, 16861 (1994).

[30]For the analytical continuation of the QMC data we used the maximum entropy method, which we cross-checked with Padé approximants.

[31]Y. Tokura, Y. Taguchi, Y. Okada, Y. Fujishima, T. Arima, K. Kumagai, and Y. Iye, Phys. Rev. Lett. **70**, 2126 (1993).

[32]P. Moetakef, C. A. Jackson, J. Hwang, L. Balents, S. J. Allen, and S. Stemmer, Phys. Rev. B **86**, 201102(R) (2012).

[33]R. Chen, S. B. Lee, and L. Balents, Phys. Rev. B **87**, 161119(R) (2013).

[34]E. Pavarini, A. Yamasaki, J. Nuss, and O. K. Andersen, New J. Phys. **7**, 188 (2005).